Vortex interactions revisited: Formation of stable elementary cells for creation of rigid vortex lattices

L. Stoyanov, N. Gorunski, M. Zhekova, I. Stefanov, A. Dreischuh

L. Stoyanov, N. Gorunski, M. Zhekova, I. Stefanov, A. Dreischuh, "Vortex interactions revisited: Formation of stable elementary cells for creation of rigid vortex lattices ," Proc. SPIE 11047, 20th International Conference and School on Quantum Electronics: Laser Physics and Applications, 110471D (29 January 2019); doi: 10.1117/12.2516531

SPIE.

Event: International Conference and School on Quantum Electronics "Laser Physics and Applications": ICSQE 2018, 2018, Nessebar, Bulgaria

Vortex interactions revisited: Formation of stable elementary cells for creation of rigid optical vortex lattices

L. Stoyanov, N. Gorunski, M. Zhekova, I. Stefanov, A. Dreischuh

Department of Quantum Electronics, Faculty of Physics,
Sofia University "St. Kliment Ohridski", Sofia-1164, Bulgaria

ABSTRACT

Optical vortices (OVs) are the only known truly two-dimensional phase dislocations. Because of their spiral phase fronts, the OV interaction results, in the simplest case (when two OVs are presented), in vortex mutual attraction/repulsion or in OV pair rotation. In this work we provide experimental evidences that a stable elementary cell forming the base for a large optical vortex lattice can be created by situating equally and singly charged OVs in the apices of a triangle and square and by nesting an additional control OV with an opposite unit charge in the center of the structure. Experimental data for the rotation of these triangular and quadratic elementary cells vs. OV-to-OV separation as well as the rotation of the same structures vs. propagation distance are presented. Generation and stable propagation of large rigid square-shaped and hexagonal OV lattices is demonstrated.

Keywords: singular optics, optical vortex, vortex lattice, topological interaction.

1. INTRODUCTION

Optical vortices (OVs) are two-dimensional singular beams with spiral phase dislocations in their wavefronts[1]. OVs carry photon angular momentum, which can also be transferred to matter and it is referred to as the topological charge (TC). The TC m is a positive or negative integer number corresponding to the total phase change $2\pi m$ over the azimuthal coordinate φ. It is known that a pair of singly and equally charged OVs placed on a bright background beam, rotate and repel each other[2,3], whereas OVs of opposite TCs translate with respect to the background beam, attract each other and eventually annihilate. In nonlinear media, these fundamental interaction scenarios remain qualitatively the same during the initial stage of nonlinear evolution, both under self-defocusing and self-focusing conditions[4]. However, at later stages of their evolution, the vortex dynamics under self-focusing conditions is additionally influenced by the reshaping of the surrounding part of the background beam[4].

For the first time the possibility to stabilize ensembles of equally-charged OVs against rotation by a proper choice of the topological charge of a "control OV" nested in the ensemble center is proved numerically in[5]. Specifically, if an OV with a TC opposite to the TCs of the rest of the OV ensemble is positioned in the center of the structure, the rotation of the entire ensemble is cancelled. An extension of such vortex ensembles towards large stable regular OV lattices is also analyzed in[5] and studied for the first time experimentally in[6].

The possibilities of singular higher-order vector fields[7] to be generated, if large and rigid OV lattices are used, along with the option to write different optically-induced parallel waveguide structures e.g. in bulk photorefractive nonlinear media[8] and their applicability e.g. for orbital angular momentum multiplexing of information[7] stimulated this work. Here we present, for the first time to our best knowledge, experimental evidences for the already adopted paradigm in singular optics: A stable elementary cell of a large optical vortex lattice can be created by situating equally and singly charged OVs in the apices of a triangle or square and nesting an additional control OV with an opposite unit charge in the center

20th International Conference and School on Quantum Electronics: Laser Physics and Applications,
edited by Tanja Dreischuh, Latchezar Avramov, Proc. of SPIE Vol. 11047, 110471D

of the structure. Experimental data for the generation of large rigid square-shaped and hexagonal OV lattices with liquid-crystal spatial light modulator are also presented.

2. EXPERIMENTAL SETUP

The experimental setup is shown in Fig. 1. Pump beam from a continuous-wave frequency-doubled Neodymium-doped yttrium orthovanadate (Nd:YVO_4) laser is first expanded by the beam expander BE and then illuminates the reflective spatial light modulator SLM at an angle of 4º vs. normal incidence. This SLM modulates the phase of the input Gaussian beam (and, as a consequence, also its amplitude/intensity). It is encoded with patterns of two (aligned in a line), three (in the apices of an equilateral triangle) or four OVs (situated in the corners of a square), all of them with the same TC=1. In some cases in the encoded phase profile we additionally imposed a central OV with an opposite TC or with same TC, as needed. This was done in order to cancel the rotation of the elementary cell or to increase it. The efficiency of the singular beam generation is 71%. The beam is then redirected towards a CCD camera with a chip of cross-section 7.1mm×5.4mm (1600 pix.×1200 pix.) by using a large-aperture beam splitter BS2. The CCD camera is placed on a rail in order to examine the rotation of these elementary cells vs. propagation distance.

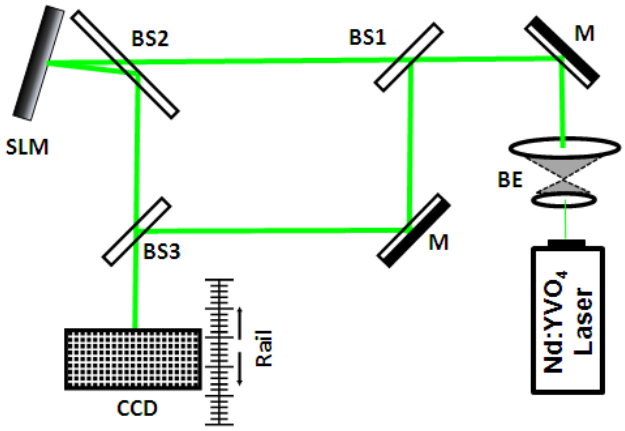

Fig. 1. Experimental setup. Nd:YVO_4, continuous-wave frequency-doubled Neodymium-doped yttrium orthovanadate laser emitting at a wavelength λ = 532 nm; BE, beam expander; M, flat silver mirrors; BS, beam splitters; SLM – reflective spatial light modulator (model Pluto, Holoeye Photonics); CCD, charge-coupled device camera placed on a rail.

For diagnostic purposes, a reference beam is split off the laser beam before the SLM by a beam splitter BS1. The object and the reference beams are recombined by another beam splitter BS3 to interfere at the CCD camera chip. Power density distributions of the resulting optical beams and the respective interference patterns are recorded by the same CCD camera by blocking/unblocking the reference laser beam. In some of the measurements presented in this work the reference arm of the interferometer is eliminated by removing BS3. In this way we studied the singular beam evolution at even shorter distances to the SLM.

3. RESULTS

The experimental results shown in the last row of Fig. 2 are intended to visualize the theoretically predicted and already mentioned basic interaction scenarios between two OVs nested on a common bright background beam[2,3]. In the upper left panel of Fig. 2 we show the well-known spiral phase profile of a singly charged OV. The directions of the vectors in the respective vector plot shown in the frame below clearly indicate its rotation on the background beam. The lower left frame in the same figure is an experimentally obtained power density distribution of such an OV. Since it does not change its position on the background beam, the dashed line crossing all experimental frames could be regarded as a reference for the rotation/translation of OV pairs of equal/opposite TCs. In the middle column of frames in Fig.2 we show that the two helical phase profiles of two equally charged OVs (upper frame) lead to an overall helicity of the phase (middle frame) and, as a consequence, to the rotation of the OV pair with respect to their “center of gravity” (lower frame). In the opposite case of OVs with TCs equal to 1 and -1, there is a phase gradient along a line perpendicular to the line connecting the OV cores (right column, vector plot). Hence, the OV pair is translating on the background beam, which is clearly seen in the experimental result (lower right frame in Fig. 2). The presented data refer to OV-to-OV separation 57 pix. on the liquid-crystal phase modulator and to a distance of linear propagation of 32 cm behind it.

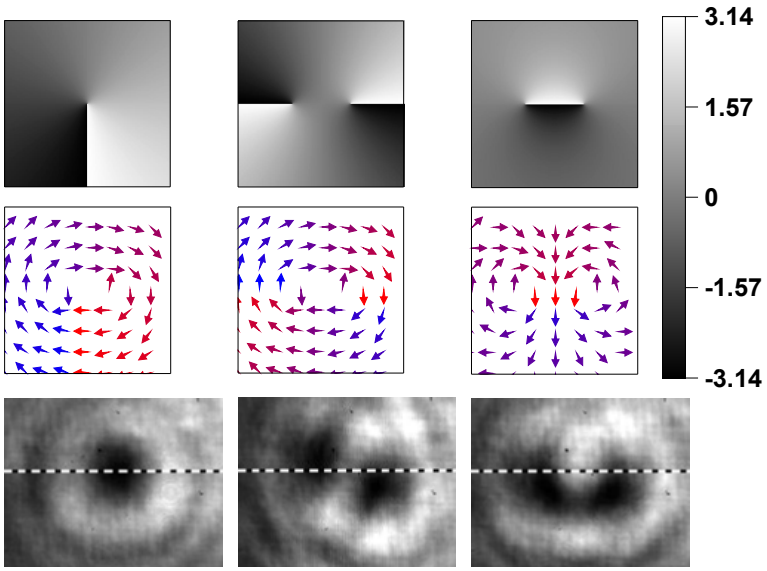

Fig. 2. Phase profiles (upper row) and vector plots (middle) of a single OV (left column), of two OVs with equal unit topological charges (middle column), and of two OVs with opposite unit topological charges (right column). Lower row – experimental data obtained at an initial OV-to-OV separation 57 pix. and at a distance of 32 cm after the SLM.

As a next step we proved experimentally that the smaller the OV-to-OV distance, the stronger pronounced interaction (in this case – rotation) is observed for structures with equally charged OVs. The obtained data shown in Fig. 3 are for a pair of OVs (crosses and dash-dotted curve), three OVs situated in the apices of an equilateral triangle (hollow triangles and dashed line) and in the apices of a square (solid squares and solid line). The measured rotation angles refer to a free space propagation distance of 32 cm. It is also clearly expressed that, at a fixed OV separation, the larger the number of equally charged OVs, the larger the rotation angle of the ensemble. This can be intuitively understood by the bigger overall helicity of the background beam.

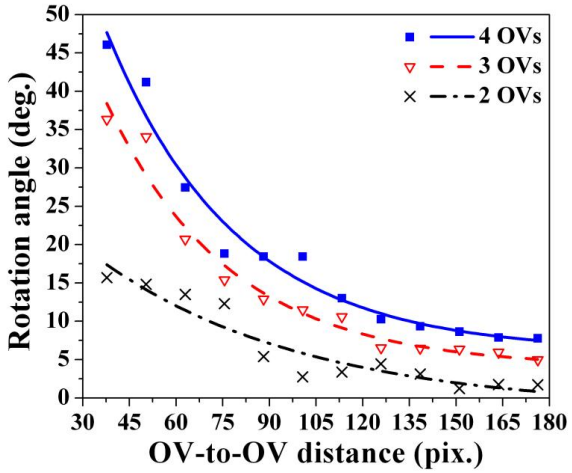

Fig. 3. Rotation of two, three and four equally and singly-charged OVs aligned in a line (crosses and dash-dotted curve), in the apices of an equilateral triangle (hollow triangles and dashed line) and in the corners of a square (solid squares and solid line), respectively, vs. OV-to-OV separation. Propagation distance – 32 cm.

In the following three sets of measurements we present data for the longitudinal increase (or stabilization) of the rotation angle of each of these ensembles separately, in the two additional cases when a control OV (with TC=±1) is nested in the center of each structure. This additionally imposed central OV is equidistant from the rest of the OVs forming the

elementary cells. The data we present in Figs. 4-6 refer to OV-to-OV separation 71 pix. on the spatial light modulator and to a propagation distance from 7 cm to 77 cm. In this sense the data for the rotation angles are directly comparable. The middle straight solid lines in Figs. 4-6 are fitting the data for the respective ensemble with no control OV. Typical power density distributions for these three cases are shown in the middle frames in the respective figures and are denoted as 2OVs, 3OVs, and 4OVs. Supported by the physical intuition one can easily understand that when an additional OV with the same TC is nested in the center of each of the ensembles, due to the increase of the overall beam helicity, the rotation of the ensembles will be accelerated. This is clearly seen in the upper curves in Figs. 4-6 fitting the experimental points in the respective cases. The fitting curves, however, are not linear anymore. This can be explained by the stronger pronounced reshaping of the surrounding background beam as compared to the case with no control OV. Another possible reason is that due to the free space propagation of the OVs in the ensemble they are starting to separate from each other, thus the interaction between them becomes weaker. This reshaping is well pronounced in the experimentally recorded intensity profiles of the respective ensembles shown in the upper frames on the right hand side of Figs. 4-6. Formally, these frames are denoted as 2OVs +, 3OVs +, and 4OVs +, respectively. In contrast, the respective experimental intensity distributions in the case for a control OV with an opposite TC are denoted as 2OVs -, 3OVs -, and 4OVs - (lower right frames in Figs. 4-6).

In the context of this paper the most important data are in the bottom of the respective graphs (linear fits denoted with dash-dotted lines). They clearly indicate the stabilization of the OV ensemble consisting of equally charged OVs when the control OV is carrying the opposite TC of the same absolute value. This is supported by the physical intuition since, because of the symmetry, the vector diagram of the "interaction forces" is closed and its vector sum is equal to zero. This should be the situation in the absence of background beam reshaping, however in the experimental data shown in the lower right frames of the respective graphs slight beam modulation occurs. That is why the rotation angles of these stabilized cases, even small, slightly differ from zero.

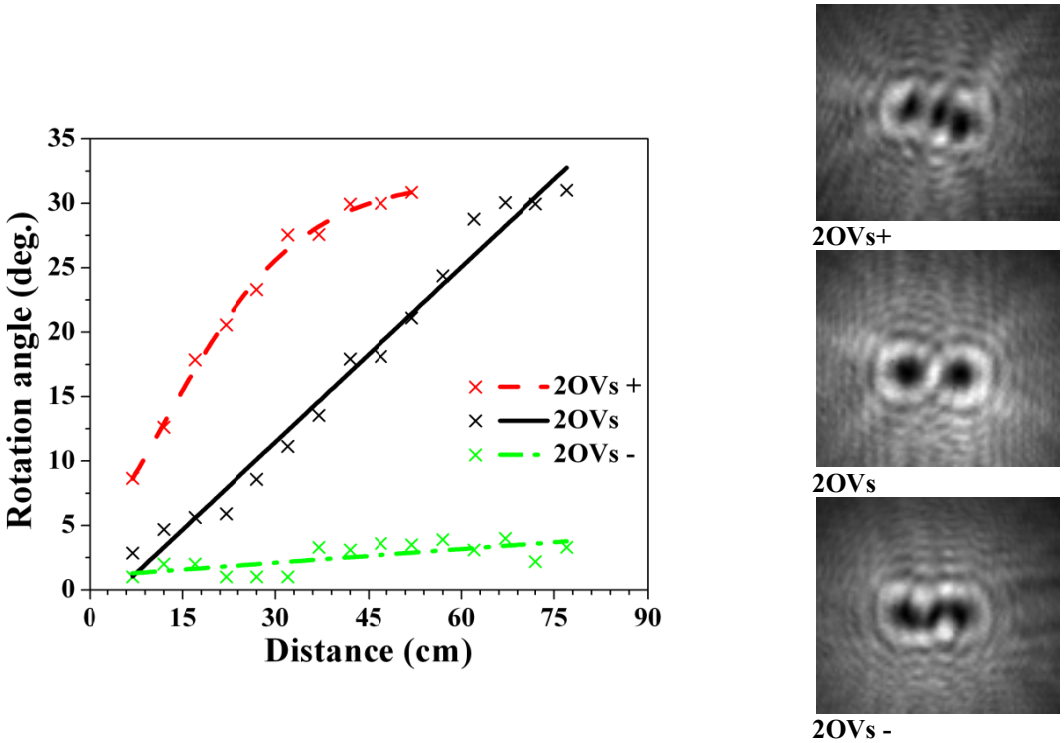

Fig. 4. **Left:** Rotation of two equally and singly-charged OVs (black crosses and solid line) vs. propagation distance. Stabilization of the OV pair rotation by an additional OV of an opposite TC (green crosses and dash-dotted line) and acceleration of this rotation by a central OV of the same TC (red crosses and dashed curve). OV-to-OV separation 71 pix. between the outer-lying OVs. **Right:** Respective experimental data recorded 17 cm after the SLM.

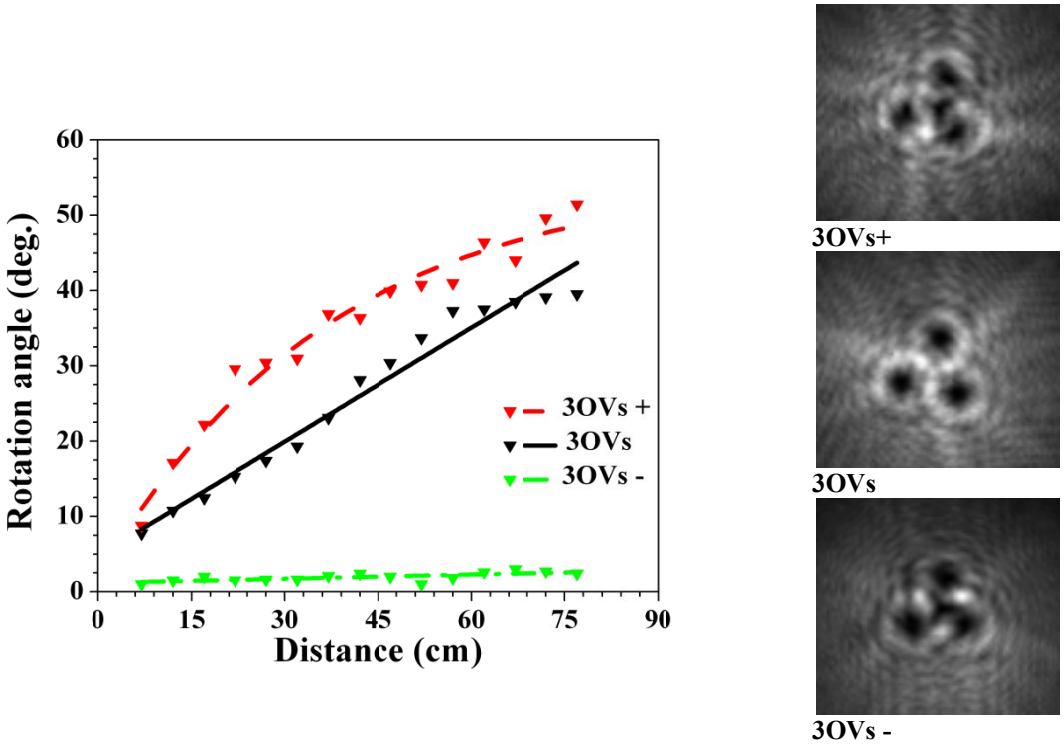

Fig.5. **Left:** Rotation of three equally and singly-charged OVs (black triangles and solid line) situated in the apices of an equilateral triangle vs. propagation distance. Stabilization of the OV ensemble rotation by an additional OV of an opposite TC in the center of the elementary cell (green triangles and dash-dotted line) and acceleration of this rotation by a central OV of the same TC (red triangles and dashed curve). OV-to-OV separation 71 pix. **Right:** Respective experimental data recorded 17 cm after the SLM.

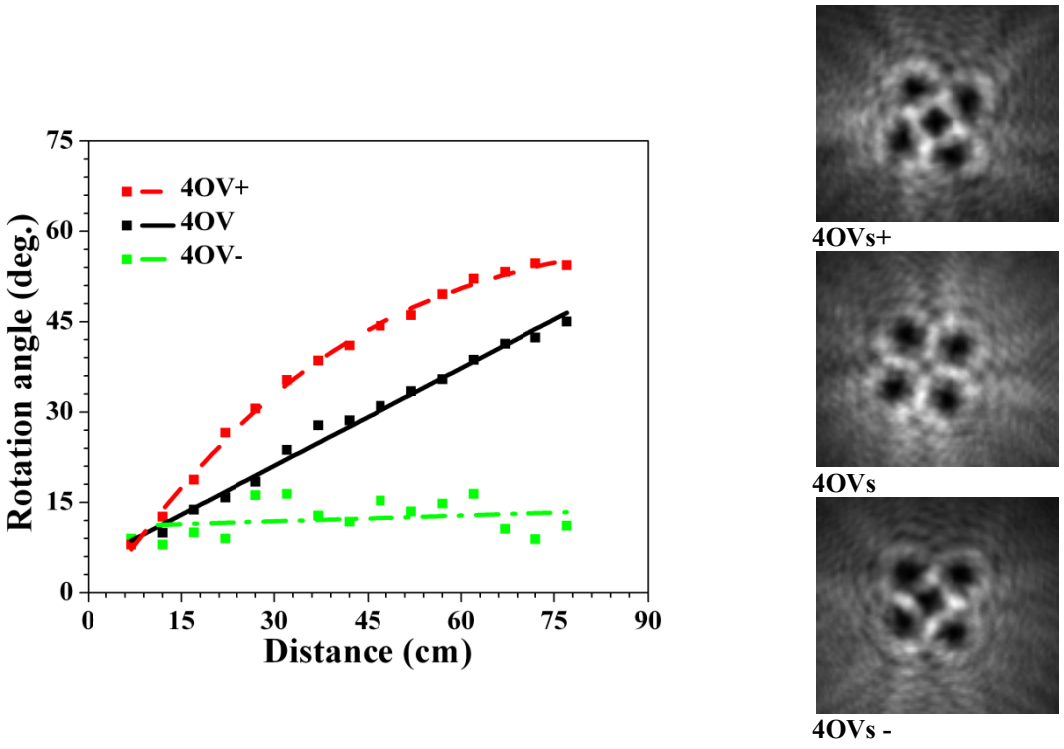

Fig.6. **Left:** Rotation of four equally and singly-charged OVs (black squares and solid line) situated in the apices of a quadrate vs. propagation distance. Stabilization of the OV ensemble rotation by an additional OV of an opposite TC in the center of the quadrate

(green squares and dash-dotted line) and acceleration of this rotation by a central OV of the same TC (red squares and dashed curve). OV-to-OV separation 71 pix. **Right:** Respective experimental data recorded 17 cm after the SLM.

In Fig. 7, in the upper row of frames we show a sketch of the elementary cell of a square-shaped OV lattice (left) and experimentally recorded intensity profiles of the central part of the square OV array at distances 7 cm (middle frame) and 27 cm behind the liquid crystal spatial light modulator (right frame). The additionally drawn dashed squares on the experimental pictures are intended to visualize the square elementary cell and the disposition of the TCs of the OVs. The TCs of two additional OVs are marked in the middle frame in this upper row in order to confirm that the square-shaped lattice can be considered as composed by vortices situated in the apices of a square with a central control OV with an opposite TC. The comparison between the positions of the OVs in the dashed squares indicates that the vortices do not change their positions and are only reshaped by the diffraction. In the lower row of frames, following the same ordering, we show a hexagonal OV lattice. Some of the topological charges of the vortices are denoted within a dashed hexagon. The TC of one additional OV is marked outside the hexagon in order to underline that identically-charged OVs situated in the apices of an equilateral triangle with a central control OV of opposite TC in the middle, form a hexagonal OV lattice with alternatively changing signs of their TCs. Once again, the comparison between the positions of the OVs in the dashed hexagons indicates that the vortices do not change their mutual positions and are only reshaped by the diffraction.

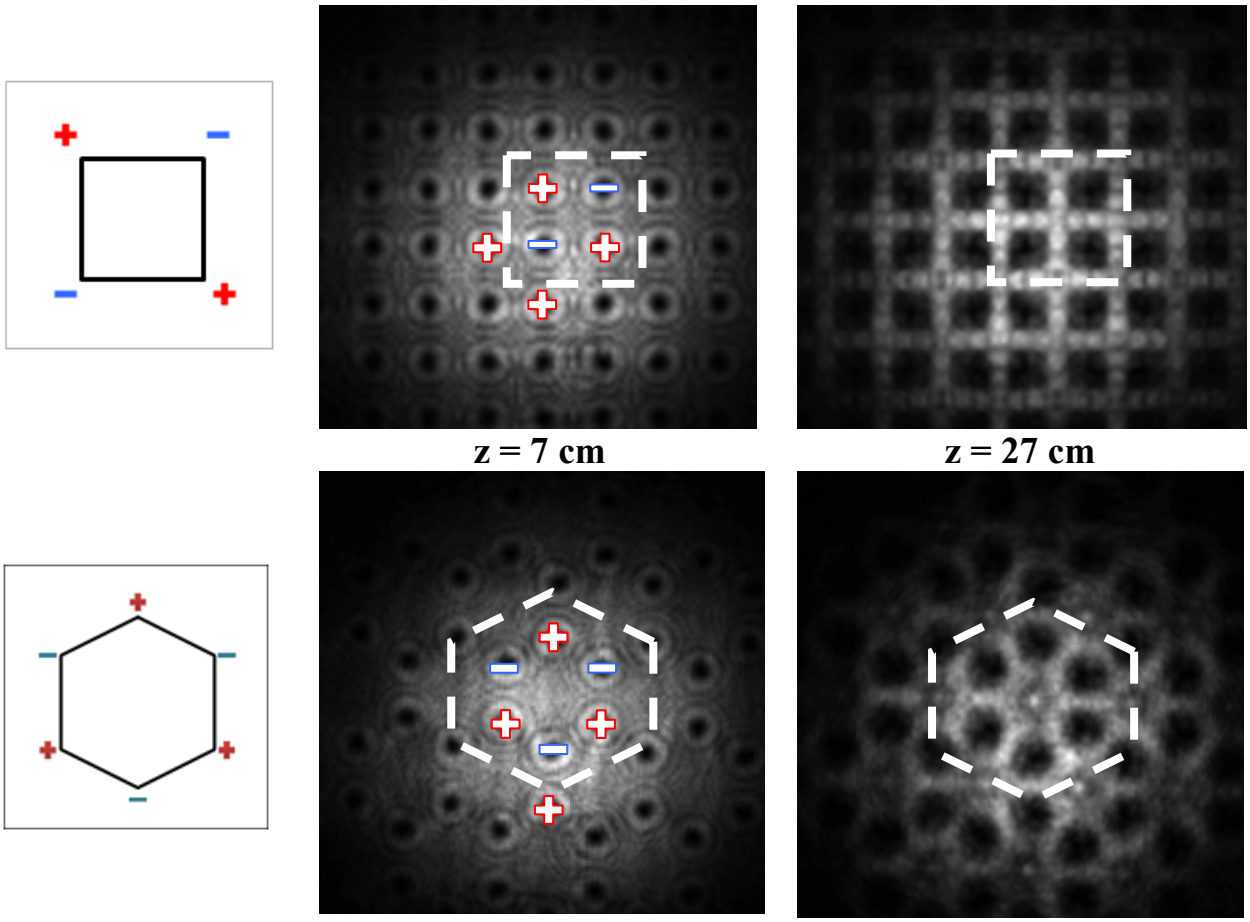

Fig. 7. **Upper row** – square-shaped OV lattice. Sketch of the lattice elementary cell with denoted signs of the TCs (left). Middle and right frames – experimentally recorded intensity profiles of the central part of the square OV array at distances 7 cm and 27 cm behind the liquid crystal spatial light modulator. **Lower row** of frames – the same, but for hexagonal OV lattice. Some of the topological charges of the vortices are denoted. See the text for details.

4. CONCLUSION

In this paper we presented, for the first time to our best knowledge, experimental evidences for the already adopted paradigm in singular optics: A stable elementary cell of a large optical vortex lattice can be created by situating equally and singly charged OVs in the apices of a triangle or square and nesting an additional control OV with an opposite unit charge in the center of the structure. On this base large OV arrays consisting of hundreds of OVs with alternating TCs are generated. In two preceding papers[9,10] we already demonstrated experimentally and by numerical calculations a dramatic far-field beam reshaping by mixing square-shaped and hexagonal optical vortex lattices. These results may appear particularly interesting, as a new degree of freedom, for modifications in stimulated emission depletion (STED) microscopy, for extending the possibilities of generating singular higher-order vector fields[7], for controllable writing of parallel optically-induced waveguide structures e.g. in (photorefractive) nonlinear media[8] and may appear applicable for orbital angular momentum multiplexing of information for data transfer using complex optical fields[11–15].

ACKNOWLEDGMENTS

We acknowledge funding of the National Science Fund (Bulgaria) within the framework of Project DFNI-T02/10-2014.

REFERENCES

[1]. Nye, J. F. and Berry, M. V., "Dislocations in wave trains," Proc. R. Soc. London Ser. A 336, 165-190 (1974).

[2]. Rozas, D., Law, C. T., and Swartzlander, Jr., G. A., "Propagation dynamics of optical vortices," J. Opt. Soc. Am. B 14, 3054-3065 (1997).

[3]. Rozas, D., Sacks, Z. S., and Swartzlander, Jr., G. A., "Experimental observation of fluidlike motion of optical vortices," Phys. Rev. Lett. 79, 3399-3402 (1997).

[4]. Hansinger, P., Dreischuh, A., and Paulus, G. G., "Optical vortices in self-focusing Kerr nonlinear media," Optics Communications 282, 3349-3355 (2009).

[5]. Neshev, D., Dreischuh, A., Assa, M., and Dinev, S., "Motion control of ensembles of ordered optical vortices generated on finite extent background," Optics Communications 151, 413-421 (1998).

[6]. Dreischuh, A., Chervenkov, S., Neshev, D., Paulus, G. G., and Walther, H., "Generation of lattice structures of optical vortices," J. Opt. Soc. Am. B 19, 550-556 (2002).

[7]. Li, S. and Wang, J., "Experimental demonstration of optical interconnects exploiting orbital angular momentum array," Optics Express 25, 21537-21547 (2017).

[8]. Stoyanov, L. Dimitrov, N. Stefanov, I., Neshev, D. N., and Dreischuh, A., "Optical waveguiding by necklace and azimuthon beams in nonlinear media," J. Opt. Soc. Am. B 34, 801-807 (2017).

[9]. Stoyanov, L., Maleshkov, G., Zhekova, M., Stefanov, I., Paulus, G. G., and Dreischuh, A., "Far-field beam reshaping by manipulating the topological charges of hexagonal optical vortex lattices," J. of Optics 20, art. No. 095601 (2018).

[10]. Stoyanov, L., Maleshkov, G., Zhekova, M., Stefanov, I., Paulus, G. G., and Dreischuh, A., "Far-field pattern formation by manipulating the topological charges of square-shaped optical vortex lattices," J. Opt. Soc. Am. B 35, 402-409 (2018).

[11]. Wang J., "Advances in communications using optical vortices," Photon. Res. 4, B14-B28 (2016).

[12]. Wang J., “Data information transfer using complex optical fields: a review and perspective,” Chinese Opt. Lett. 15, 030005 (2017).

[13]. Wang J., "Metasurfaces enabling structured light manipulation: advances and perspectives," Chinese Opt. Lett. 16, 050006 (2018).

[14]. Wang, A., Zhu, L., Wang, L., Ai, J., Chen, S., and Wang J., "Directly using 8.8-km conventional multi-mode fiber for 6-mode orbital angular momentum multiplexing transmission," Opt. Express 26, 10038-10047 (2018).

[15]. Liu, J., Li, S.-M., Zhu, L., Wang, A.-D., Chen, S., Klitis, C., Du, C., Mo, Q., Sorel, M., Yu, S.-Y., Cai, X.-L., and Wang J., "Direct fiber vector eigenmode multiplexing transmission seeded by integrated optical vortex emitters," Light: Science and Applications 7, 17148 (2018).